Internal forces in nondegenerate two-dimensional electron systems

C. Fang-Yen* and M. I. Dykman
Department of Physics and Astronomy, Michigan State University, East Lansing, Michigan 48824

M. J. Lea
Department of Physics, Royal Holloway, University of London, Egham, Surrey TW20 0EX, England
(Received 21 June 1996; revised manuscript received 3 February 1997)

We use Monte Carlo (MC) simulations to study the Coulomb forces that drive individual electrons in a two-dimensional normal electron fluid and a Wigner crystal. These forces have been previously shown to determine many-electron magnetoconductivity and cyclotron resonance of nondegenerate electron systems; they are also known to provide an important characteristic of the dynamics of particles that form a fluid. We have calculated the moments of the force distribution that are relevant for electron transport, which will permit a quantitative comparison of the many-electron transport theory with experiment. We have investigated the shape of the force distribution. Far tails of the distribution were analyzed by combining the method of optimal fluctuation with MC calculations, and the results were compared with direct MC results. [S0163-1829(97)05424-6]

I. INTRODUCTION

Much work has been done in the past few years on many-electron effects in nondegenerate two-dimensional (2D) electron systems on the surface of liquid helium and in semiconductors. For electron densities n_s and temperatures T investigated experimentally, the ratio of the Coulomb energy of electron-electron interaction to T is usually large, $\Gamma \gtrsim 10$, where

$$\Gamma = e^2(\pi n_s)^{1/2}/T. \tag{1}$$

Therefore the electron system is strongly correlated. It is a normal electron fluid in which the wave functions of different electrons do not overlap, or for $\Gamma \gtrsim 127$ (lower T), a Wigner crystal.

Most studies of many-electron effects in nondegenerate systems have dealt with various types of plasma waves,[1–3] and the Wigner transition and collective excitations in a Wigner crystal.[4–10] However, except for Monte Carlo analyses of the velocity autocorrelation function,[11] the dynamics of electrons in a normal fluid remains unexplored. This is related to the absence of ''good'' quasiparticles — the problem generally encountered in the physics of liquids.

An important characteristic of electron dynamics in a normal fluid and in a crystal, is the internal force on an electron or, equivalently, the electric field $\mathbf{E}_f$ that drives each electron due to thermal fluctuations of electron density. The field $\mathbf{E}_f$ (and the force $e\mathbf{E}_f$) is essentially all that an electron ''knows'' about other electrons at a given time provided the variation of the field across the electron wavelength $\lambda\!\!\!^{-}$ is small compared to the field itself:

$$\lambda\!\!\!^{-}|\langle \nabla_n \mathbf{E}_n \rangle| \ll \langle E_f^2 \rangle^{1/2}, \tag{2}$$

where $\mathbf{E}_n$ is the field on the nth electron. The condition (2) means that the motion of an electron in the field of other electrons is classical or, in the presence of a quantizing magnetic field, semiclassical.[12]

Internal forces have attracted much attention in the physics of liquids.[13] They are particularly interesting in the case of a 2D electron fluid, since they can be used[12] to describe, in a broad parameter range, magnetoconductivity, the cyclotron resonance spectrum, and other magnetotransport phenomena which are commonly investigated in experiment to characterize electron systems. The theory[12] relates magnetotransport coefficients to the characteristic function of the distribution of the field $\mathbf{E}_f$ and to the moments of this distribution. However, theoretical analysis of the field $\mathbf{E}_f$ has been done so far only for the harmonic Wigner crystal.

In this paper we present results of a Monte Carlo (MC) investigation of the fluctuational internal field in the broad range $10 \leqslant \Gamma \leqslant 200$ that includes the normal electron fluid, Wigner crystal, and the phase transition between the two. Extensive MC simulations of nondegenerate 2D electron systems were first performed in the late 70s and early 80s (Refs. 11,14–17) (see Ref. 18 for a review; for more recent work see for example Refs. 9,19,20 and references therein). However, the fluctuational field was not analyzed, and the distribution of the field cannot be obtained from the cited results. Our results will further be used to perform detailed qualitative and quantitative comparison of the many-electron transport theory with experiment in Ref. 21.

In Sec. II we formulate the problem of the fluctuational field and briefly discuss the MC algorithm. In Sec. III we present results for scaled $\langle E_f^2 \rangle$ and $\langle E_f^{-1} \rangle$ as functions of the single parameter Γ. We also discuss singular behavior of internal energy, self-diffusion, and $\langle E_f^2 \rangle$ near the melting transition. In Sec. IV we combine the method of optimal fluctuation and the Monte Carlo method to find the logarithm of the distribution, which is then compared with direct calculations of Sec. III. Section V contains concluding remarks.

II. FORMULATION OF THE PROBLEM

The Coulomb field $\mathbf{E}_n$ on the nth electron is determined by the positions $\{\mathbf{r}_{n'}\}$ of all electrons in the system

$$\mathbf{E}_n \equiv \mathbf{E}_n(\{\mathbf{r}_{n'}\}) = -\frac{1}{e}\nabla_n H_{\rm ee},$$

$$H_{\rm ee} = \frac{1}{2}e^2 {\sum_{n,n'}}' |\mathbf{r}_n - \mathbf{r}_{n'}|^{-1}. \quad (3)$$

For classical electron systems the distribution $\rho(\mathbf{E}_f)$ of the field on an electron is given by the expression

$$\rho(\mathbf{E}_f) = Z_c^{-1} \int \left(\prod d\mathbf{r}_{n'}\right) \delta[\mathbf{E}_f - \mathbf{E}_n(\{\mathbf{r}_{n'}\})] e^{-H_{\rm ee}/T},$$

$$Z_c = \int \left(\prod d\mathbf{r}_{n'}\right) \exp(-H_{\rm ee}/T). \quad (4)$$

Clearly, the form of the distribution does not depend on the number n of an electron in (3),(4).

It is convenient to change to dimensionless variables

$$\mathbf{r}_n \to e\mathbf{r}_n n_s^{3/4} T^{-1/2}, \quad \mathbf{E}_f \to \mathbf{E}_f/E_0, \quad E_0 = n_s^{3/4} T^{1/2}. \quad (5)$$

The distribution of the dimensionless field $\mathbf{E}_f/E_0$ is seen from (3), (4) to be determined by the single parameter Γ.

The quantity E_0 provides the characteristic scale of the fluctuational field. This is seen, e.g., from the expression for the mean square field $\langle E_f^2 \rangle$ in terms of the two-particle distribution function of the electron system $\mathcal{P}(\mathbf{r}_1, \mathbf{r}_2)$:

$$e^2\langle E_f^2 \rangle \equiv \langle (\nabla_n H_{\rm ee})^2 \rangle = -eT\langle \nabla_n \mathbf{E}_n \rangle = \frac{e^2 T}{n_s S} \int \frac{\mathcal{P}(\mathbf{r}_1, \mathbf{r}_2)}{|\mathbf{r}_1 - \mathbf{r}_2|^3} d\mathbf{r}_1 d\mathbf{r}_2, \quad (6)$$

where S is the area of the system. For a normal fluid the function $\mathcal{P}(\mathbf{r}_1, \mathbf{r}_2)$ depends on $|\mathbf{r}_1 - \mathbf{r}_2|$, i.e., $\mathcal{P}(\mathbf{r}_1, \mathbf{r}_2) = n_s^2\, g(|\mathbf{r}_1 - \mathbf{r}_2|)$, where $g(r)$ is the pair correlation function. If the interparticle distance is scaled by $n_s^{-1/2}$, then the ratio $H_{\rm ee}/T$, which determines the form of $g(r)$, depends only on Γ and the scaled particle coordinates. Therefore the correlation function $g(r)$ depends only on the scaled distance $r n_s^{1/2}$ and Γ, i.e., $g(r) = \tilde{g}(r n_s^{1/2}; \Gamma)$. As $r \to \infty$ the function $g(r)$ approaches 1, whereas for $r \ll n_s^{-1/2}$ it becomes very small. It follows from (6), therefore, that

$$\langle E_f^2 \rangle = F(\Gamma) E_0^2 \equiv F(\Gamma) n_s^{3/2} T. \quad (7)$$

For a Wigner crystal one can approximate

$$\mathcal{P}(\mathbf{r}_1, \mathbf{r}_2) \approx {\sum_{n,n'}}' \delta(\mathbf{r}_1 - \mathbf{R}_n)\, \delta(\mathbf{r}_2 - \mathbf{R}_{n'})$$

($\mathbf{R}_n$ are the lattice sites) which gives the asymptotic value of $F(\Gamma)$

$$F_W = n_s^{-3/2} {\sum_{n}}' |\mathbf{R}_n - \mathbf{R}_0|^{-3}. \quad (8)$$

For a triangular lattice $F_W \approx 8.91$.[22]

It follows from (7), (8) that in the range (2) we have the inequality

$$e\langle E_f^2 \rangle^{1/2} \lambda\!\!\!^{-} \ll T, \quad (9)$$

which is the criterion for applicability of the classical approximation (4).[23] [For zero or classically strong magnetic fields the characteristic wavelength $\lambda\!\!\!^{-} = \lambda\!\!\!^{-}_T \equiv \hbar/(2mT)^{1/2}$.]

It can be shown[12] that in the range (9), Eq. (4) applies also for quantizing magnetic fields. The characteristic wavelength in this case is given by

$$\lambda\!\!\!^{-} = l_B(2\overline{n} + 1)^{-1/2}, \quad l_B = (\hbar/m\omega_c)^{1/2},$$

$$\omega_c = eB/m, \quad \overline{n} = [\exp(\hbar\omega_c/T) - 1]^{-1}. \quad (10)$$

It is seen from (10) that in a strong quantizing field B, where $\overline{n} \ll 1$, the wavelength $\lambda\!\!\!^{-} \ll \lambda\!\!\!^{-}_T$. Therefore, even for $e\langle E_f^2 \rangle^{1/2} \lambda\!\!\!^{-}_T > T$, where the electron motion is no longer classical in the absence of the magnetic field, the criterion (9) may still apply. This means that, by using a magnetic field, one may substantially broaden the range of electron densities and temperatures over which the effects of electron-electron interaction on the electron dynamics may be analyzed in terms of internal forces.

Monte Carlo algorithm

The integral (4) was evaluated using the Metropolis algorithm.[24] We modeled the system as a fixed number of electrons placed on a rectangular unit cell with periodic boundary conditions and neutralized by a uniform positive background. The aspect ratio of the unit cell and the number of particles in the cell N were chosen so as to be able to accommodate a perfect triangular lattice:[14]

$$L_y/L_x = \sqrt{3}/2, \quad N = 4M^2, \text{ with integer } M. \quad (11)$$

Following Ref. 14, we used the Ewald summation technique to evaluate the potential of an electron and its infinite set of images, minus the corresponding potential of the positive background. The electric field of an electron and its images was evaluated as a numerical gradient of the potential, which proved to be more computationally efficient than a direct Ewald summation. The potential and electric field components at a point $\mathbf{r} \equiv (x,y)$ due to an electron at $x = y = 0$ were tabulated on a 200×200 grid in the region $x/L_x \in (0, 0.5)$, $y/L_y \in (0, \sqrt{3}/4)$ (by symmetry it was only necessary to consider one-fourth of the unit cell). This grid was used for four-point interpolation[25] during the simulation. In order to improve interpolation accuracy at small distances, the radially symmetric singular terms (r^{-1} and r^{-2} for the potential and field, respectively) were subtracted prior to tabulation and added during the simulation. This allowed an efficient determination of the potential with an error of less than 0.005%.

We ran simulations with $N = 100$, 144, 256, and 324. We found good convergence of all characteristics investigated as a function of N; there are $1/N$ corrections to the moments of the field $\mathbf{E}_f$ related to the motion of the center of mass of the system. The data presented in this paper is for $N = 256$, which seemed to represent a reasonable compromise between a large number of particles and the amount of computer time needed to run the simulation.

The particles were initially placed either in a random configuration or a perfect triangular lattice. During each MC step, one electron was chosen at random and a displacement

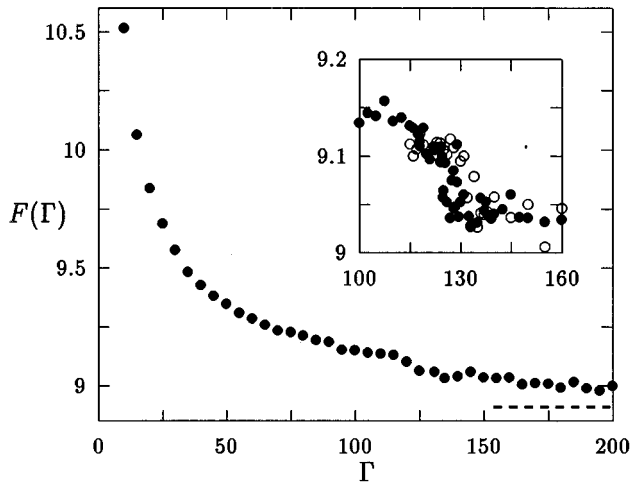

FIG. 1. Scaled mean square fluctuational field $F(\Gamma)=\langle E_f^2\rangle/n_s^{3/2}T$. The asymptotic value F_W for a harmonic Wigner crystal is shown dashed. Inset: $F(\Gamma)$ near the melting transition, for crystalline (●) and random (○) initial configurations.

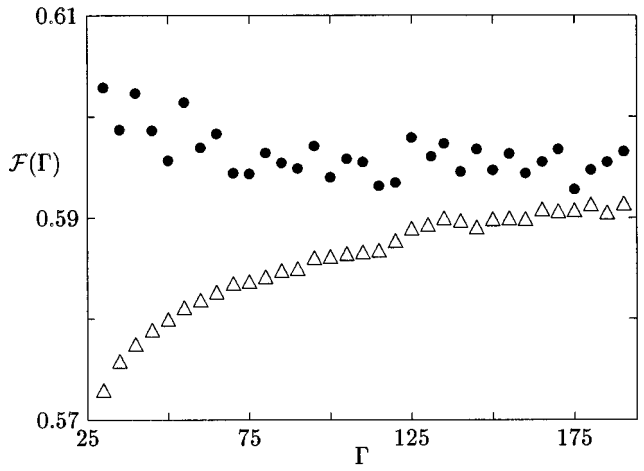

FIG. 2. Scaled mean reciprocal field $\mathcal{F}(\Gamma)=n_s^{3/4}T^{1/2}\langle E_f^{-1}\rangle$ (●) and its value if the field distribution were Gaussian, $[\pi/F(\Gamma)]^{1/2}$ (△).

was considered within a square of side length $2\delta_{\rm MC}$ centered about the particle's position. The value of $\delta_{\rm MC}$ was chosen so that approximately 50% of attempts were accepted, which provides the fastest convergence. The corresponding value is $\delta_{\rm MC}^{(0)}\approx 0.848e^{-1}n_s^{-3/4}T^{1/2}$.

In each of our runs the number of MC steps (per particle) exceeded 50 000. (We note that the total number of steps $\sim 10^7$ is very small compared to the period of our nonlinear additive feedback random number generator.) For values of Γ away from the phase transition the first $\approx$20 000 steps were discarded in order to allow the system to come to equilibrium (or quasiequilibrium). This number was obtained from the data on the decay of systematic drift in the total energy of the system, which proved to be a relatively slowly converging quantity. The vicinity of the phase transition is discussed in Sec. III A.

Our results for the radial distribution function are in good agreement with Ref. 14.

III. MOMENTS OF THE FLUCTUATIONAL FIELD

The MC results for the scaled mean square fluctuational field $F(\Gamma)$ (7) are shown in Fig. 1. For $\Gamma\gtrsim 10$, the function F decreases monotonically with increasing Γ. Quite remarkably, the variation of F is small in the whole range $\Gamma\gtrsim 10$, although the structure of the system changes dramatically, from a liquid where correlations in electron positions decay within twice the mean electron separation, to a crystal. The function $F(\Gamma)$ appears to have a smeared singularity at the melting point $\Gamma\approx 127$. This is further discussed in Sec. III A.

The behavior of the function F can be qualitatively understood by noting that, due to the weighting factor $|\mathbf{r}_1-\mathbf{r}_2|^{-3}$ in the integral (6), $\langle E_f^2\rangle$ is determined primarily by short-range order in the system. Therefore the value of $\langle E_f^2\rangle$ for an electron liquid at large Γ would be expected to be close to that for a Wigner crystal. Variation of the scaled field $F(\Gamma)$ with Γ for an electron liquid is determined by the structure of the correlation function $g(|\mathbf{r}_1-\mathbf{r}_2|)\equiv n_s^{-2}\mathcal{P}(\mathbf{r}_1,\mathbf{r}_2)$. With decrease of Γ the peaks of $g(r)$ are broadened. If we assume the broadening occurs symmetrically, it is clear that because of the weight r^{-3}, the ''gain'' in the integral (6) due to the increased small-r tail is slightly greater than the ''loss'' due to the increased large-r tail. Therefore the overall effect of the changes in $g(r)$ is a slow increase of F as Γ decreases.

For a Wigner crystal, the decrease of $F(\Gamma)$ with increasing Γ can be seen from Eq. (6) written in the form

$$F(\Gamma)=n_s^{-5/2}S^{-1}{\sum_{n,n'}}'\ \langle|\mathbf{R}_n-\mathbf{R}_{n'}+\mathbf{u}_n-\mathbf{u}_{n'}|^{-3}\rangle$$

$$\approx\frac{1}{n_sS}{\sum_{n,n'}}'\ n_s^{-3/2}|\mathbf{R}_n-\mathbf{R}_{n'}|^{-3}\left(1+\frac{9}{4}\frac{\langle|\mathbf{u}_n-\mathbf{u}_{n'}|^2\rangle}{|\mathbf{R}_n-\mathbf{R}_{n'}|^2}\right),$$

where $\mathbf{u}_n$ is the displacement of the nth electron from its equilibrium position. The temperature-dependent correction in the right-hand side is $\propto\Gamma^{-1}$. We note that the divergence of the mean square displacement does not affect the validity of the above expansion, because $\langle|\mathbf{u}_n-\mathbf{u}_{n'}|^2\rangle$ increases only logarithmically, as $\Gamma^{-1}n_s^{-1}\ln|\mathbf{R}_n-\mathbf{R}_{n'}|$, for large $|\mathbf{R}_n-\mathbf{R}_{n'}|$.

In the limit of small Γ the major contribution to the field $\mathbf{E}_f$ comes from pair collisions; when two electrons come to within a distance $r\sim e^2/T\ll n_s^{-1/2}$ the squared field on each of them increases as r^{-4}. A straightforward calculation in which one ignores the effect of other electrons on the colliding electrons gives

$$F(\Gamma)\approx 2\pi^{3/2}\Gamma^{-1},\quad \Gamma\ll 1. \tag{12}$$

Extrapolating the estimate (12) to $\Gamma\sim 1$ gives $F(1)\approx 11$, which approximately matches the value of $F(1)$ obtained from MC (not shown in Fig. 1).

The variation of the scaled mean reciprocal field $\mathcal{F}=E_0\langle E_f^{-1}\rangle$ with Γ is shown in Fig. 2. The function $\mathcal{F}$ decreases monotonically with increasing Γ. As in the case of the scaled mean square field F, the overall variation in $\mathcal{F}$ in

the range $\Gamma \gtrsim 10$ is small. If the distribution of the fluctuational field were Gaussian, $\mathcal{F}$ would be related to F by

$$\mathcal{F}(\Gamma) = E_0 \langle E_f^{-1} \rangle|_{\text{Gauss.}} \Rightarrow [\pi/F(\Gamma)]^{1/2}. \tag{13}$$

The distribution of the field is indeed Gaussian for a harmonic Wigner crystal, which is a standard result for the distribution of the force driving a particle in a classical solid (we note that, in contrast to the mean square displacement from the lattice site, which diverges for $T>0$, the mean square force remains finite in a 2D crystal). In a fluid this distribution is close to Gaussian for large Γ, because for most of the time, electrons perform vibrations about quasiequilibrium positions with small amplitudes $\sim \Gamma^{-1/2} n_s^{-1/2} \ll n_s^{-1/2}$. As Γ decreases, vibrations become increasingly anharmonic and the deviation from Gaussian becomes more substantial. (The exact shape of the distribution will be discussed in the next section.) Therefore the difference between $\mathcal{F}$ and $(\pi/F)^{1/2}$ increases as well. In contrast to $\mathcal{F}$, the function $(\pi/F)^{1/2}$ increases monotonically with Γ.

It is seen from Fig. 2 that the spread of the data points for the scaled reciprocal field $\mathcal{F}$ is larger than for F. We attribute this to the contribution from electron configurations where the field on an electron is substantially less than the mean square root field.

The decrease of $\mathcal{F}$ with Γ can be easily understood for small Γ. In this case, electrons move nearly independently from each other, and for most of the time the field on an electron is $\sim e n_s$, and correspondingly $\mathcal{F} \sim \Gamma^{-1/2}$. These arguments seem to differ from those used in the analysis of $\langle E_f^2 \rangle$ where it was important to allow for occasional pair collisions in which the field was very strong. Such collisions do not contribute to $\langle E_f^{-1} \rangle$.

Vicinity of the melting transition

We identified the position of the melting point by the change of the internal energy and onset of self-diffusion in the electron system. The internal potential energy is given by the expression

$$U = \frac{1}{2} e^2 \int \frac{\mathcal{P}(\mathbf{r}_1, \mathbf{r}_2) - n_s^2}{|\mathbf{r}_1 - \mathbf{r}_2|} d\mathbf{r}_1 d\mathbf{r}_2. \tag{14}$$

It is convenient to consider a reduced average potential energy per electron

$$\mathcal{U} = e^{-2} (\pi n_s)^{-1/2} \left[\left(\frac{U - U_W}{n_s S} \right) - T \right], \tag{15}$$

where U_W is the potential energy U for a triangular lattice, $U_W \approx -1.96 e^2 n_s^{3/2} S$.[26] The term T is subtracted in (15) to allow for the mean thermal potential energy of electron vibrations in the harmonic approximation.

The results for $\mathcal{U}$ vs Γ are shown in Fig. 3. When the initial configuration of electrons was a perfect crystal the function $\mathcal{U}$ was found to vary smoothly with increasing Γ except in the range $125 \lesssim \Gamma \lesssim 130$ where $\mathcal{U}$ drops sharply. This is consistent with a first-order phase transition smeared by finite-size effects. On the lower ''branch'' of $\mathcal{U}$ ($\mathcal{U} \lesssim 0.0005$) the electron system displays crystalline order, whereas on the upper branch of $\mathcal{U}$ it is disordered. In several runs the average energy took on an intermediate value between the branches. The corresponding electron configurations displayed various degrees of disorder.

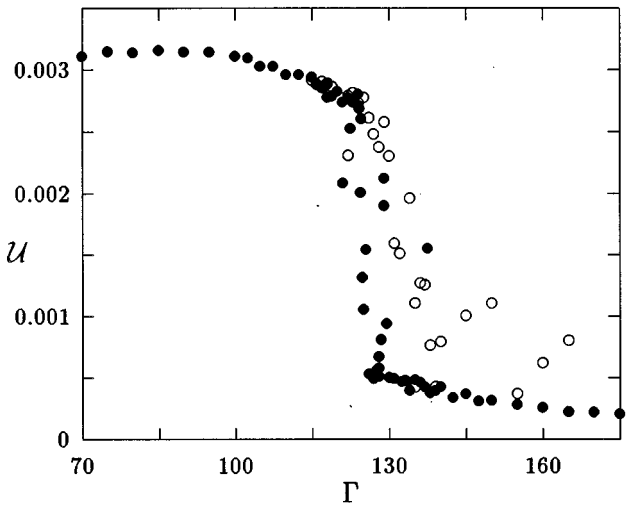

FIG. 3. Reduced mean electron potential energy $\mathcal{U}$ (15) vs Γ for crystalline (●) and random (○) initial configurations.

The Metropolis algorithm does not provide direct data on the dynamics of the system. However, it still can be used to qualitatively characterize the diffusion in a relatively narrow temperature range where the characteristic microscopic ''attempt'' frequencies remain nearly constant. An effective diffusion constant D as a function of Γ was obtained as follows: after allowing the system to reach equilibrium, we measured the displacements $\Delta(K)$ of particles as a function of the number K of MC steps per particle, up to $K \approx 50\,000$. We found that $\langle \Delta^2(K) \rangle \propto K$ for large K. That is, the displacement of electrons is diffusionlike, and we can define a dimensionless diffusion coefficient $D = \langle \Delta^2(K) \rangle / (K \delta_{\text{MC}}^2)$. We verified the independence of D on the step size δ_{MC} in the range $0.1 < \delta_{\text{MC}} / \delta_{\text{MC}}^{(0)} < 1.2$.

We found that for runs in which the initial configuration of the electrons was a perfect crystal, the diffusion coefficient was very small for $\Gamma \geqslant 130$ and was due to the translation of the finite-size crystal as a whole. The parameter D increased by a factor of ~ 15 when Γ decreased from 130 to 126 and increased smoothly as Γ was further lowered. This, as well as the data on the electron energy $\mathcal{U}$, indicate a melting point of the Wigner crystal at $\Gamma_m \approx 127 \pm 2$, in agreement with experimental results[5] and previous computer simulations.[14,15]

In the transition region, the melting of initially crystallized electrons sometimes required more than the 20 000 MC steps normally used to equilibrate the system. In these cases D was determined by considering the diffusion only after melting had occurred. The number of MC steps used to calculate D in every case exceeded 20 000.

For runs which started with random initial configurations, the values of the reduced potential energy $\mathcal{U}$ and the diffusion coefficient D for $\Gamma < 125$ were approximately equal to $\mathcal{U}$ and D for runs in which the system was initially a crystal. This was no longer true for larger Γ. For random initial configurations the value of D was larger than for crystalline

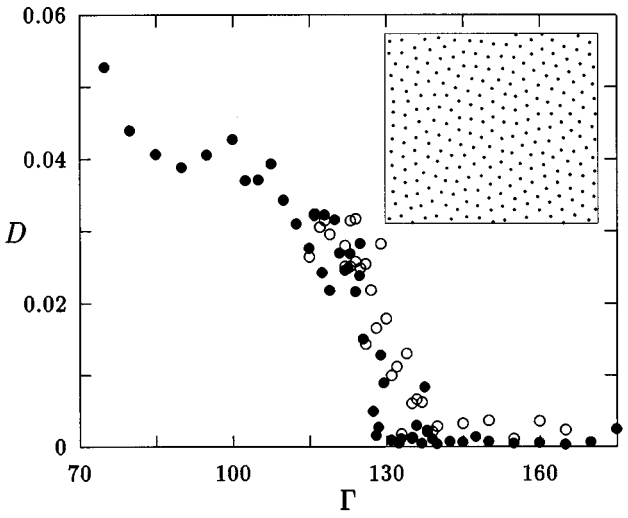

FIG. 4. Effective diffusion constant D vs Γ in the region of the melting transition for crystalline (●) and random (○) initial configurations. Inset: Snapshot of a disordered configuration for $\Gamma=130$.

initial configurations in the range $\Gamma\lesssim 140$. Comparatively large values of D in the range $\Gamma\lesssim 132$ for initially disordered configurations suggest that the disordered state is metastable in this range of $\Gamma>\Gamma_m$. A snapshot of the system in a metastable state is shown in the inset of Fig. 4.

Metastability of the disordered state is supported also by the data on the energy $\mathcal{U}$. Arguably, the dependence of $\mathcal{U}$ on Γ displays hysteresis for Γ close to Γ_m; the values of $\mathcal{U}$ are larger for the disordered state. For larger $\Gamma-\Gamma_m$ the state with long-range translational order is expected to be the only stable state of the system. However, because of the extremely small diffusion coefficients for respective temperatures, in particular for $\Gamma>140$, some defects (such as dislocation pairs) remained quenched when the system was initially disordered, even with the maximum number of MC steps used in the simulation. (Diffusion of defects and the effect of boundaries on the defect energies were discussed in Ref. 27). This is clearly seen from the final configurations of the system. As a result, the energy of the initially disordered system remained larger than that of the initially crystalline one; cf. Fig. 3.

We note the similarity between the expression (6) for the scaled mean square fluctuational field $F\propto\langle\mathbf{E}_f^2\rangle$ and the expressions (14), (15) for $\mathcal{U}$. If the liquid-crystal transition is first order, we should expect both $\mathcal{U}$ and F to be discontinuous; therefore experimental investigation of F may shed light on the order of the transition. Our data for F in Fig. 1 shows what is arguably a smeared discontinuity when the Wigner crystal is melted, with F greater on the liquid side of the transition, similar to $\mathcal{U}$. The values of F are slightly larger for random rather than crystalline initial configurations. We note that the spread of the data is relatively large in the vicinity of the transition.

The behavior of the internal energy, field, and diffusion with varying Γ suggests that melting of a Wigner crystal is a first order transition. This conclusion coincides with that of Kalia *et al.*[17] based on molecular dynamics simulations of the many-electron system. Our value for the entropy change per particle at melting $\Delta S\approx 0.28k_B$ is close to the result of Ref. 17 $\Delta S\approx 0.3k_B$ and the prediction of the mean-field theory[28] $\Delta S\approx 0.32k_B$. We note that our results have been obtained using a different MC technique than in Ref. 17. The other difference is that in Ref. 17 hysteresis was investigated by monotonically heating Wigner crystal or cooling electron liquid, whereas in our case the data were obtained starting each time from a crystalline or random configuration, independently for each Γ. In contrast to Ref. 17 we have observed configurations with metastable defects.

The entropy change on melting $\Delta S\approx 0.28k_B$ may be also compared to an upper limit for the change of entropy on melting of $0.2k_B$ for electrons on helium found experimentally in Ref. 29. We note that the data in Ref. 29 was obtained in a range where quantum effects should be taken into account in the analysis of electron motion in the field of other electrons. These effects lie outside the scope of the present paper.

In the range below $\Gamma\approx 126$ we observed a smooth dependence of $\mathcal{U}$ on Γ, down to $\Gamma=10$. A recent estimate[30] of the value of Γ_h for the hexatic phase to liquid transition, which was obtained assuming two-stage melting, gives $24.5<\Gamma_h<104.85$. Within the accuracy of our calculations for the internal energy, we found no evidence for such a transition. Detailed data on melting of a 2D Wigner crystal will be discussed elsewhere.

IV. LOGARITHM OF THE FIELD DISTRIBUTION

The logarithm of the probability density distribution of one of the field components, $\rho(E_{fx})$, for two values of Γ is shown in Fig. 5. The logarithm of the field is parabolic near the minimum in the investigated range $\Gamma\geqslant 10$, which corresponds to the central part of the distribution being Gaussian. The deviation from Gaussian shape as characterized by the fourth moment was small; we found that the ratio $[\langle E_{fx}^4\rangle-\frac{3}{4}\langle E_f^2\rangle^2]/\langle E_f^2\rangle^2$ was ≈ 0.1 for $\Gamma=10$ and decreased to 0.03 for $\Gamma>100$. The mean reciprocal field $\langle E_f^{-1}\rangle$ also is seen from Fig. 2 to be close to its value for a Gaussian distribution.

For an electron fluid the distribution of different components of the field should be the same. We verified that $\rho(E_{fx})=\rho(E_{fy})$ in the liquid phase, within the accuracy of the data. For a Wigner crystal with sixfold symmetry we expect that $\langle E_{fx}^2\rangle=\langle E_{fy}^2\rangle$, $\langle E_{fx}^4\rangle=\langle E_{fy}^4\rangle=3\langle E_{fx}^2E_{fy}^2\rangle$. These relations held true to within an accuracy of $\sim 2\%$. We have also analyzed the sixth moments of the components. These moments should reflect the difference between the isotropic electron fluid and Wigner crystal. For example, $[\langle E_{fx}^2E_{fy}^4\rangle-(1/16)\langle E_f^6\rangle]/[(1/16)\langle E_f^6\rangle]$ should be equal to zero in a fluid, and is in general nonzero in a crystal. However, in the simulations it was as small as $\lesssim 0.02$ for a crystal. This shows that the anisotropy of the central part of the field distribution in a Wigner crystal is small.

It is seen from Fig. 5 that in the far tails the distribution decays much slower than a Gaussian distribution with the same width; the dependence of the logarithm of the probability distribution on E_{fx} goes from parabolic to nearly linear for large $E_{fx}/\langle E_f^2\rangle^{1/2}$. The tails are determined by the prob-

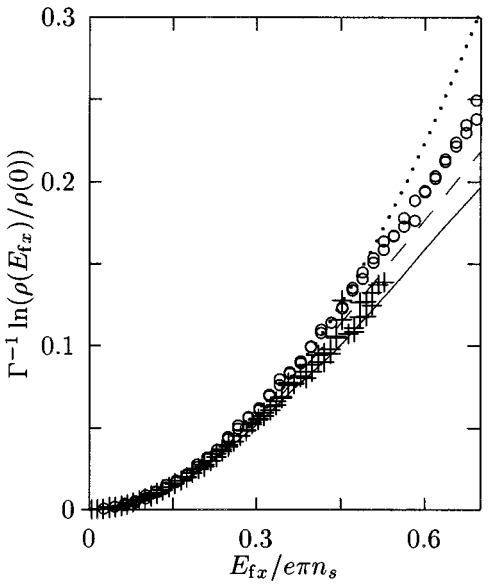

FIG. 5. Logarithm of the distribution of the field component $\rho(E_{fx})$ as a function of the scaled field $E_{fx}/e\pi n_s$ for $\Gamma=60$ (+) and 20 (○). Solid and dashed lines show the results obtained by the method of optimal fluctuation for x and y components of the field, respectively. Dotted line refers to a Gaussian distribution for the harmonic Wigner crystal. The data points extend to the far tails of the distribution where $E_{fx}^2/\langle E_f^2\rangle \approx 11$ for $\Gamma=60$, and $E_{fx}^2/\langle E_f^2\rangle \approx 5.5$ for $\Gamma=20$.

abilities of large electron displacements from quasiequilibrium positions.

The shape of the tails for comparatively large Γ can be investigated analytically using the method of optimal fluctuation. The small probability that the field $\mathbf{E}_n$ on the nth electron takes on a given large value $\mathbf{E}_f$ ($E_f \gg \langle E_f^2\rangle^{1/2}$) is determined by the probability of the optimal (least improbable) fluctuation that gives rise to such a field. Fluctuation probabilities are given by the factor $\exp(-H_{ee}/T)$. Therefore, the dominant term in the logarithm of the probability density of the corresponding optimal fluctuation can be found from the minimal value of H_{ee}/T for which $\mathbf{E}_n = \mathbf{E}_f$,

$$-\ln[\rho(\mathbf{E}_f)/\rho(0)] \approx (H_{ee}^{(f)}[\mathbf{E}_f] - H_{ee}^{(f)}[0])/T, \qquad H_{ee}^{(f)}[\mathbf{E}_f] \equiv H_{ee}(\{\mathbf{r}_{n'}^{(f)}\}),\ \ \mathbf{E}_n \equiv \mathbf{E}_n(\{\mathbf{r}_{n'}^{(f)}\}) = \mathbf{E}_f. \tag{16}$$

The optimal electron positions $\mathbf{r}_{n'}^{(f)}$ for a given field $\mathbf{E}_f$ and the minimal value $H_{ee}(\{\mathbf{r}_{n'}^{(f)}\})$ are given by the solution of the variational problem

$$H_{ee}(\{\mathbf{r}_{n'}^{(f)}\}) = \min[H_{ee}(\{\mathbf{r}_{n'}\}) - \boldsymbol{\lambda}(\mathbf{E}_n(\{\mathbf{r}_{n'}\}) - \mathbf{E}_f)],$$

which is reduced to a set of algebraic equations

$$\frac{\partial}{\partial \mathbf{r}_{n'}}[H_{ee}(\{\mathbf{r}_{n'}\}) - \boldsymbol{\lambda}\mathbf{E}_n(\{\mathbf{r}_{n'}\})] = 0, \qquad \mathbf{E}_n(\{\mathbf{r}_{n'}\}) \equiv -e^{-1}\nabla_n H_{ee}(\{\mathbf{r}_{n'}\}) = \mathbf{E}_f. \tag{17}$$

Here, $\boldsymbol{\lambda}$ is the Lagrange multiplier. Clearly, the value of $H_{ee}(\{\mathbf{r}_{n'}^{(f)}\})$ is independent of the number n of the electron for which the field $\mathbf{E}_n$ is considered (but the positions $\mathbf{r}_{n'}^{(f)}$ depend on n). The value $H_{ee}[0]$ is the minimal Coulomb energy for $\mathbf{E}_n = \mathbf{E}_f = 0$. The configuration $\mathbf{r}_{n'}^{(f)}$ for $E_f = 0$ corresponds to lattice sites of a Wigner crystal: $\mathbf{r}_{n'}^{(0)} = \mathbf{R}_{n'}$.

The problem (17) can be solved analytically for small $\mathbf{E}_f$. In this case the optimal positions $\mathbf{r}_{n'}^{(f)}$ correspond to small displacements $\mathbf{u}_{n'}$ of the electrons from lattice sites $\mathbf{R}_{n'}$. The displacements can be found by expanding H_{ee} and $\mathbf{E}_n$ to second and first order in $\mathbf{u}_{n'}$, respectively, in which case (17) becomes a set of linear equations for $\mathbf{u}_{n'}$. The displacements $\mathbf{u}_{n'}$ are proportional to $\mathbf{E}_f$, and the resulting increment in H_{ee} is quadratic in $\mathbf{E}_f$. One can show that in this approximation

$$\frac{H_{ee}^{(f)}[\mathbf{E}_f] - H_{ee}^{(f)}[0]}{T} = \pi^{3/2}\Gamma\frac{E_f^2}{E_R^2 F_W}, \quad E_R = e\pi n_s. \tag{18}$$

The parameter F_W is defined in (8) and is expressed in terms of a lattice sum.

Equation (18) applies for $E_f \ll E_R$ where anharmonic terms in the expansion of H_{ee} in $\mathbf{u}_{n'}$ are small. However, for large Γ the ratio (18) may be large even for small E_f/E_R. It is seen from (7), (8), (18) that

$$\pi^{3/2}\Gamma\frac{E_f^2}{E_R^2 F_W} = \frac{E_f^2}{\langle E_f^2\rangle_W},$$

where $\langle E_f^2\rangle_W$ is the mean square field for a harmonic Wigner crystal. This shows that the method of optimal fluctuation correctly describes the Gaussian distribution of the field on a particle in the range of comparatively strong fields where $\langle E_f^2\rangle^{1/2} \lesssim E_f \ll E_R$.

In the range $E_f \sim E_R$ (and $E_f > E_R$) the logarithm of the field distribution $\rho(\mathbf{E}_f)$ as given by (16), (17) becomes nonparabolic in $\mathbf{E}_f$ and anisotropic: it depends on the orientation of $\mathbf{E}_f$ with respect to the lattice vectors of the Wigner crystal. The variational problem for $\rho(\mathbf{E}_f)$ in the range $E_f \gtrsim E_R$ can be analyzed numerically.

Numerical solution of Eq. (17) for the many-electron system was obtained from MC simulation of an auxiliary system with the Hamiltonian

$$\widetilde{H}_{ee} = H_{ee}(\{\mathbf{r}_{n'}\}) - \boldsymbol{\lambda}\mathbf{E}_n(\{\mathbf{r}_{n'}\}).$$

We used the same algorithm as in the MC simulations of the real system, with particles initially arranged in a crystal configuration. The simulations were done with extremely small effective temperatures in order to find the ground state configuration of the auxiliary system for a given $\boldsymbol{\lambda}$. By varying $\boldsymbol{\lambda}$ we obtained different values of the fluctuational field $\mathbf{E}_f$ and found the corresponding energies $H_{ee}^{(f)}[\mathbf{E}_f]$.

The results for $\Gamma^{-1}\ln[\rho(\mathbf{E}_f)/\rho(0)]$ obtained from the numerical solution of the variational problem are plotted in Fig. 5. Note from (16) that $\Gamma^{-1}\ln[\rho(\mathbf{E}_f)/\rho(0)]$ for optimal fluctuations is independent of temperature and is a function of the scaled field $\mathbf{E}_f/E_R$ only. We analyzed orientations of $\mathbf{E}_f$ in the x and y directions, which are the directions to the nearest and next nearest neighbors, respectively [we note that

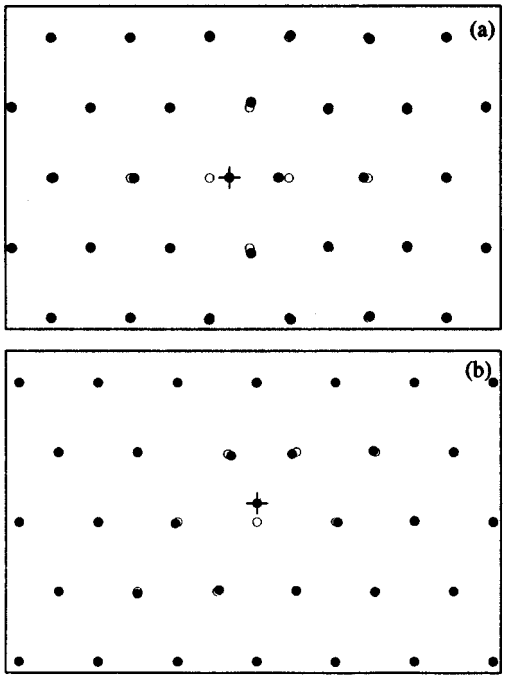

FIG. 6. Optimal electron positions (full circles) for a strong field $\mathbf{E}_f$ in the x (a) and y (b) directions. The particle that experiences the field is marked by a cross. Lattice sites are shown by empty circles.

the orientation of the crystal is fixed by the choice of aspect ratio (11) of the rectangle containing the electrons].

The optimal electron configurations for the fields E_{fx} and E_{fy} are shown in Fig. 6. The optimal configuration for the force eE_x on a given particle corresponds to the displacements towards each other of this particle and its nearest neighbor in the x direction. Two nearby particles are displaced by small amounts away from the given particle, as shown. In the case of a force eE_y, the optimal configuration corresponds to the displacement of the particle in the y direction, while the closest neighbors on its way move towards each other in the x direction. The displacements of the other particles are small in both cases and decay within a few interparticle distances.

It is seen from Fig. 5 that optimal fluctuations which give rise to a field of a given amplitude in the direction of a nearest neighbor are more probable than for a field in a perpendicular direction, as would be expected. In both cases the dependence of $\ln\rho(\mathbf{E}_f)$ on $\mathbf{E}_f$ changes from parabolic to nearly linear with increasing E_f, and the crossover occurs in the range $0.3<E_f/E_R<0.4$. The slopes of $\ln\rho(\mathbf{E}_f)$ in the quasilinear region are nearly equal for different orientations of $\mathbf{E}_f$.

The distribution of the field component in the nearest-neighbor direction obtained from direct MC simulations is seen in Fig. 5 to be close to the results obtained by the method of optimal fluctuation over the entire range of fields we investigated. As expected, the agreement is particularly good for large Γ where the method of optimal fluctuation applies immediately. It follows from Fig. 5 that $\Gamma=60$ is sufficiently large, but the agreement is still reasonably good even for $\Gamma=20$ where the oscillations of the pair correlation function for the electron fluid decay over three mean interparticle distances. As expected, for smaller Γ fluctuations that give rise to a given large E_f/E_R are ''less optimal,'' and thus less probable. We note that $\langle E_f^2\rangle/E_R^2=\pi^{-3/2}F(\Gamma)/\Gamma\lesssim 2\Gamma^{-1}$ increases quickly with decreasing Γ, and therefore for smaller Γ it was possible to analyze the distribution over a broader range of E_f/E_R.

V. CONCLUSIONS

We have investigated internal fluctuational forces that drive electrons in a nondegenerate 2D electron system and found the distribution of the scaled fluctuational field $\mathbf{E}_f/n_s^{3/4}T^{1/2}$ on an electron as a function of the plasma parameter Γ. The results refer to the range $10\leqslant\Gamma\leqslant 200$, where the electron system varies from a normal electron fluid with the correlation length of two mean interelectron distances to a Wigner crystal, including the region of the melting transition. We have analyzed the moments of the fluctuational field $\langle E_f^2\rangle$ and $\langle E_f^{-1}\rangle$, quantities which determine magnetoconductivity and cyclotron resonance of a nondegenerate many-electron system in strong magnetic fields. The variation of the moments of the scaled field $\mathbf{E}_f/n_s^{3/4}T^{1/2}$ throughout the range $10\leqslant\Gamma\leqslant 200$ was found to be relatively small, $\approx 15\%$. The central part of the distribution of $\mathbf{E}_f$ is close to Gaussian. These results indicate that, to a substantial extent, in the range $\Gamma>10$ electron motion is nearly harmonic vibrations about quasiequilibrium positions.

The tails of the distribution of the field $\mathbf{E}_f$ are non-Gaussian, and are anisotropic for a Wigner crystal. Direct MC data and data obtained by the method of optimal fluctuation are in good quantitative agreement in a broad range of $\mathbf{E}_f/n_s^{3/4}T^{1/2}$, where the distribution varies by several orders of magnitude. The logarithm of the distribution of $\mathbf{E}_f$ is close to linear on the far tails. The anisotropy of the slope of the logarithm of the field distribution is small.

The results of this paper make it possible to perform a quantitative comparison of the many-electron theory of magnetotransport with experiment and to describe the experimental data in a broad range of the magnetic field, electron density, and temperature. Detailed experimental data on magnetoconductivity of a normal electron fluid will be presented and compared with the theory in Ref. 21.

We note that if Wigner crystallization is a first order transition, the moments of the field $\mathbf{E}_f$, and thus the magnetotransport coefficients, should be discontinuous at the melting point. However, from MC simulations we expect the discontinuity to be small ($\sim 1\%$). For electrons on helium the Debye temperature of a Wigner crystal for $B=0$ is close numerically to the melting temperature T_m, and the semiclassical approximation used to obtain the MC data does not apply. Comparison of experimental results with the theory should be done therefore when the temperature sweeps through T_m in a sufficiently strong magnetic field such that $\hbar e^2\langle E_f^2\rangle/m\omega_c\ll T^2$, since in this case the motion of electrons may be well described in the semiclassical approximation.

ACKNOWLEDGMENTS

C.F.Y. acknowledges financial support from the Department of Physics at Stanford University, and the Center for Fundamental Material Research and REU program at MSU.

*Now at Department of Physics, MIT, Cambridge, MA 02139.
[1] C.C. Grimes and G. Adams, Phys. Rev. Lett. **36**, 145 (1976); C.C. Grimes, Surf. Sci. **73**, 379 (1978).
[2] D.B. Mast, A.J. Dahm, and A.L. Fetter, Phys. Rev. Lett. **54**, 1706 (1985); D.C. Glattli, E. Andrei, G. Deville, J. Pointrenaud, and F.I.B. Williams, *ibid.* **54**, 1710 (1985); P.J.M. Peters, M.J. Lea, A.M.L. Janssen, A.O. Stone, W.P.N.M. Jacobs, P. Fozooni, and R.W. van der Heijden, *ibid.* **67**, 2199 (1991); O.I. Kirichek, P.K.H. Sommerfeld, Yu.P. Monarhka, P.J.M. Peters, Yu.Z. Kovdrya, P.P. Steijaert, R.W. van der Heijden, and A.T.A.M. de Waele, *ibid.* **74**, 1190 (1995).
[3] A.L. Fetter, Phys. Rev. B **32**, 7676 (1985); **33**, 3717 (1986); **33**, 5221 (1986); S.S. Nazin and V.B. Shikin, Sov. Phys. JETP **67**, 288 (1988); V.A. Volkov and S.A. Mikhailov, *ibid.* **67**, 1639 (1988); I.L. Aleiner and L.I. Glazman, Phys. Rev. Lett. **72**, 2935 (1994).
[4] C.C. Grimes and G. Adams, Phys. Rev. Lett. **42**, 795 (1979); D.S. Fisher, B.I. Halperin, and P.M. Platzman, *ibid.* **42**, 798 (1979).
[5] G. Deville, J. Low Temp. Phys. **72**, 135 (1988); M.A. Stan and A.J. Dahm, Phys. Rev. B **40**, 8995 (1989).
[6] V.M. Pudalov, M.D'Iorio, S.V. Kravchenko, and J.W. Campbell, Phys. Rev. Lett. **70**, 1866 (1993); G.M. Summers, R.J. Warburton, J.G. Michels, R.J. Nicholas, J.J. Harris, and C.T. Foxon, *ibid.* **14**, 2150 (1993).
[7] E.Y. Andrei, Physica B **197**, 335 (1994) and references therein.
[8] See, e.g., I.V. Kukushkin, V.I. Fal'ko, R.J. Haug, K. von Klitzing, K. Eberl, and K. Tötemayer, Phys. Rev. Lett. **72**, 3594 (1994); A.A. Shashkin, V.T. Dolgopolov, G.V. Kravchenko, M. Wendel, R. Schuster, J.P. Kotthaus, R.J. Haug, K. von Klitzing, K. Ploog, H. Nickel, and W. Schlapp, *ibid.* **73**, 3141 (1994) and references therein.
[9] M.-C. Cha and H.A. Fertig, Phys. Rev. Lett. **74**, 4867 (1995).
[10] K. Shirahama and K. Kono, Phys. Rev. Lett. **74**, 781 (1995); A. Kristensen, K. Djerfi, P. Fozooni, M.J. Lea, P.J. Richardson, A. Santrich-Badal, A. Blackburn, and R.W. van der Heijden, *ibid.* **77**, 1350 (1996).
[11] J.P. Hansen, D. Levesque, and J.J. Weis, Phys. Rev. Lett. **43**, 979 (1979); R.K. Kalia, P. Vashishta, S.W. de Leeuw, and A. Rahman, J. Phys. C **14**, L991 (1981).
[12] M.I. Dykman, in *2D Electron Systems on Helium and Other Substrates*, edited by E.Y. Andrei (Kluwer, Dordrecht, 1997); M.I. Dykman, C. Fang-Yen, and M.J. Lea, preceding paper, Phys. Rev. B **55** 16 249 (1997).
[13] C.A. Croxton, *Liquid State Physics — a Statistical Mechanical Introduction* (Cambridge University Press, Cambridge, England, 1974).
[14] R.C. Gann, S. Chakravarty, and G.V. Chester, Phys. Rev. B **20**, 326 (1979).
[15] R.H. Morf, Phys. Rev. Lett. **43**, 931 (1979).
[16] H. Totsuji and H. Kakeya, Phys. Rev. A **22**, 1220 (1980).
[17] R.P. Kalia, P. Vashishta, and S.W. de Leeuw, Phys. Rev. B **23**, 4794 (1981); P. Vashishta and R.K. Kalia, in *Melting, Localization, and Chaos*, edited by R.K. Kalia and P. Vashishta (Elsevier, New York, 1982), p. 43.
[18] K.J. Strandburg, Rev. Mod. Phys. **60**, 161 (1988).
[19] R. Price and P.M. Platzman, Phys. Rev. B **44**, 2356 (1991).
[20] V.M. Bedanov and F.M. Peeters, Phys. Rev. B **49**, 2667 (1994).
[21] M.J. Lea, P. Fozooni, A. Kristensen, P.J. Richardson, K. Djerfi, M.I. Dykman, C. Fang-Yen, and A. Blackburn, following paper, Phys. Rev. B **55**, 16 280 (1997).
[22] M.I. Dykman, J. Phys. C **15**, 7397 (1982).
[23] L.D. Landau and E.M. Lifshitz, *Statistical Physics*, 3rd ed., Pt. 1 (Pergamon, New York, 1980).
[24] N. Metropolis, A.W. Rosenbluth, M.N. Rosenbluth, A.M. Teller, and E. Teller, J. Chem. Phys. **21**, 1087 (1953).
[25] *Handbook of Mathematical Functions*, edited by M. Abramowitz and I.M. Stegun (Dover, New York, 1970).
[26] L. Bonsall and A.A. Maradudin, Phys. Rev. B **15**, 1959 (1977).
[27] D.S. Fisher, B.I. Halperin, and R.H. Morf, Phys. Rev. B **20**, 4692 (1979).
[28] T.V. Ramakrishnan, Phys. Rev. Lett. **48**, 541 (1982).
[29] D.C. Glattli, E.Y. Andrei, and F.I.B. Williams, Phys. Rev. Lett. **60**, 420 (1988).
[30] V.N. Ryzhov and E.E. Tareyeva, Phys. Rev. B **51**, 8789 (1995).